nature chemical biology

ARTICLE

PUBLISHED ONLINE: 22 DECEMBER 2013 | DOI: 10.1038/NCHEMBIO.1429

Integrated phenotypic and activity-based profiling links Ces3 to obesity and diabetes

Eduardo Dominguez[1], Andrea Galmozzi[1], Jae Won Chang[1], Ku-Lung Hsu[1], Joanna Pawlak[1], Weiwei Li[1], Cristina Godio[1], Jason Thomas[1], David Partida[1], Sherry Niessen[1], Paul E O'Brien[2], Aaron P Russell[3], Matthew J Watt[4], Daniel K Nomura[1], Benjamin F Cravatt[1]* & Enrique Saez[1]*

Phenotypic screening is making a comeback in drug discovery as the maturation of chemical proteomics methods has facilitated target identification for bioactive small molecules. A limitation of these approaches is that time-consuming genetic methods or other means are often required to determine the biologically relevant target (or targets) from among multiple protein-compound interactions that are typically detected. Here, we have combined phenotypic screening of a directed small-molecule library with competitive activity-based protein profiling to map and functionally characterize the targets of screening hits. Using this approach, we identify carboxylesterase 3 (Ces3, also known as Ces1d) as a primary molecular target of bioactive compounds that promote lipid storage in adipocytes. We further show that Ces3 activity is markedly elevated during adipocyte differentiation. Treatment of two mouse models of obesity-diabetes with a Ces3 inhibitor ameliorates multiple features of metabolic syndrome, illustrating the power of the described strategy to accelerate the identification and pharmacologic validation of new therapeutic targets.

Phenotypic screening is seeing a renaissance in drug discovery as the target-focused approaches that have dominated the industry over the past several decades have yet to translate into a greater number of new medicines[1]. A recent survey of all first-in-class small-molecule medications approved between 1999 and 2008 has shown that, only 17 (34%) came from target-based approaches as compared to 28 (56%) derived from phenotypic screens[2]. In a target-oriented campaign, molecules are optimized on a single protein that is hypothesized to have a critical role in the disease in question. The advantages of this approach are clear: screens with greater throughput can be developed, and concrete measures of target modulation provide a rational path to optimize leads. The drawbacks of a target-centric strategy are that interaction of a compound with a single protein may not be sufficient to elicit a therapeutic response *in vivo* and that insufficient knowledge of the mechanism of action can result in unexpected toxicity or lack of efficacy for the optimized drug candidate. These limitations are particularly evident in metabolic disease indications, where therapeutic outcome reflects a complex interplay across multiple organs.

In contrast, phenotypic screening aims to identify compounds that induce a desirable biological response without making *a priori* assumptions about the underlying molecular target (or targets). Phenotypic screening thus provides a less biased approach to chemically interrogate the proteome in its native context and increases the likelihood of uncovering new biology as well as small molecules that modulate targets that are part of dynamic complexes and signaling pathways. As a result, bioactive molecules isolated in phenotypic screens could be viewed as being more likely to have therapeutic impact *in vivo*. Phenotypic screening hits may also constitute better starting points for optimization as they must be cell permeable and engage their targets with sufficient affinity to displace endogenous interacting metabolites or proteins. Some of the disadvantages of phenotypic screening are that the assays have lower throughput and must serve as robust surrogates for the desired outcome *in vivo*. However, the greatest challenge of phenotypic screens is arguably the identification of the molecular targets of bioactive small molecules. Without a target (or targets), optimization and preclinical development of phenotypic hits are challenging tasks.

Advances in chemical proteomics, genomics and informatics are beginning to provide tools to overcome the hurdle of target identification for phenotypic screening hits[3–7]. Traditional affinity chromatography, in which the bioactive molecule is coupled to a solid matrix and used to pull down interacting proteins, has benefitted greatly from the development of more sensitive and quantitative proteomic approaches (for example, stable isotope labeling by amino acids in cell culture (SILAC))[8,9]. Nonetheless, validation of the molecular target from a list of interacting proteins still requires further genetic, chemical and/or biophysical methods.

Activity-based protein profiling (ABPP) is a chemical proteomics approach that exploits the conserved mechanistic and/or structural features of large enzyme families to develop chemical probes that irreversibly bind their active sites[10,11]. An activity-based probe consists of a reactive group that interacts with the active sites of proteins coupled to a reporter tag that can be used to visualize probe-labeled enzymes by SDS-PAGE (for example, rhodamine) or to enrich and identify these proteins using avidin-biotin and MS-based proteomics methods, respectively. ABPP has been used to comparatively profile enzyme activities across different types of cells, tissues and disease states[10]. When performed in a competitive mode, ABPP can also identify the target (or targets) to which a small-molecule inhibitor binds directly in native cell and tissue proteomes[12]. This feature can lead to the rapid identification of the molecular target of bioactive compounds emerging from phenotypic screens.

Here, we tested whether competitive ABPP could hasten the identification of targets of small molecules that show activity in a cell-based assay measuring differentiation and lipid accumulation

[1]Department of Chemical Physiology and The Skaggs Institute for Chemical Biology, The Scripps Research Institute, La Jolla, California, USA. [2]Centre for Obesity Research and Education–Monash University, The Alfred Hospital, Prahran, Australia. [3]Centre for Physical Activity and Nutrition Research School of Exercise and Nutrition Sciences, Deakin University, Burwood, Australia. [4]Biology of Lipid Metabolism Laboratory, Department of Physiology, Monash University, Clayton, Victoria, Australia. *e-mail: cravatt@scripps.edu or esaez@scripps.edu

in adipocytes, readouts that can serve to identify molecules of potential value as insulin sensitizers *in vivo*[13]. Insulin resistance and type 2 diabetes are characterized by increased levels of plasma free fatty acids and ectopic lipid deposition[14]. Thus, agents that restore normal tissue lipid partitioning often enhance insulin sensitivity. To increase the probability of success, we employed a small-molecule library and competitive ABPP probes directed to interact with serine hydrolases, a large and diverse class of enzymes that has important roles in mammalian metabolism and includes members with validated therapeutic potential in diabetes and obesity[15,16]. A subset of bioactive compounds identified in the screen was found by competitive ABPP to target the serine hydrolase Ces3 in mouse adipocytes. Administration of one of these Ces3 inhibitors to high fat–fed or obese-diabetic *db/db* mice protected them from weight gain, improved blood lipid levels and increased insulin sensitivity and glucose tolerance. We also found that the activity of human CES1 (hCES1, the ortholog of mouse Ces3) is elevated in adipose tissue of humans with obesity and type 2 diabetes. These data show that phenotypic screening of directed small-molecule libraries paired with cognate probes for competitive ABPP can facilitate rapid identification and *in vivo* validation of the molecular target of bioactive compounds of potential therapeutic relevance to metabolic disease.

RESULTS

Profile of serine hydrolase activity during adipogenesis

To pilot the integration of cell-based screening with competitive ABPP as an approach to discover new metabolic drug targets,

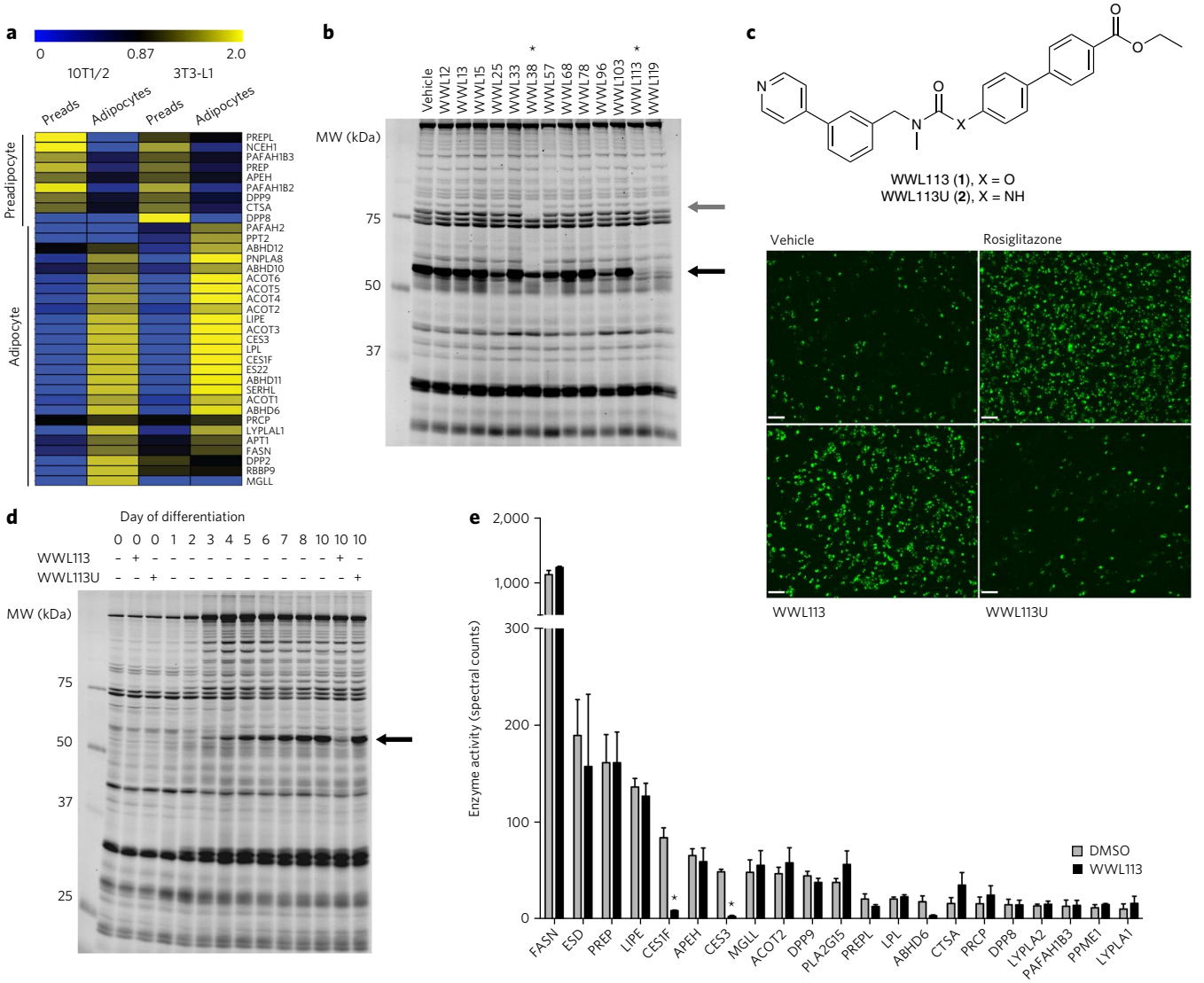

Figure 1 | Discovery of serine hydrolase inhibitors with adipogenic activity and identification of their molecular target. (**a**) Hierarchical cluster analysis of serine hydrolase signals detected by ABPP-MudPIT in 3T3-L1 and 10T1/2 preadipocyte and adipocyte proteomes. Data represent the normalized mean of three independent experiments. (**b**) Gel-based competitive ABPP analysis of adipocyte 10T1/2 cells labeled *in situ* with carbamates that promote differentiation and lipid accumulation in fat cells. A ~60-kDa serine hydrolase (black arrow) is inhibited by multiple pro-adipogenic carbamates. WWL38 inhibits HSL (gray arrow); WWL113 appears specific for the 60-kDa activity. Image is representative of two independent experiments. MW, molecular weight. (**c**) Structure of WWL113 and its urea derivative (WWL113U). WWL113, but not WWL113U, promotes adipocyte formation and lipid storage in 10T1/2 cells. Green fluorescence corresponds to Nile red staining. Images are representative of ten independent experiments. Scale bars, 250 μm. (**d**) Competitive ABPP shows that WWL113 selectively targets a ~60-kDa serine hydrolase activity that is highly induced during differentiation of 10T1/2 adipocytes; WWL113U has no effect. Image is representative of three independent experiments. (**e**) Competitive ABPP-MudPIT analysis of proteomes from 10T1/2 adipocytes incubated with WWL113 reveals that this compound is a Ces3 and Ces1f inhibitor. Error bars represent s.d. (n = 3).

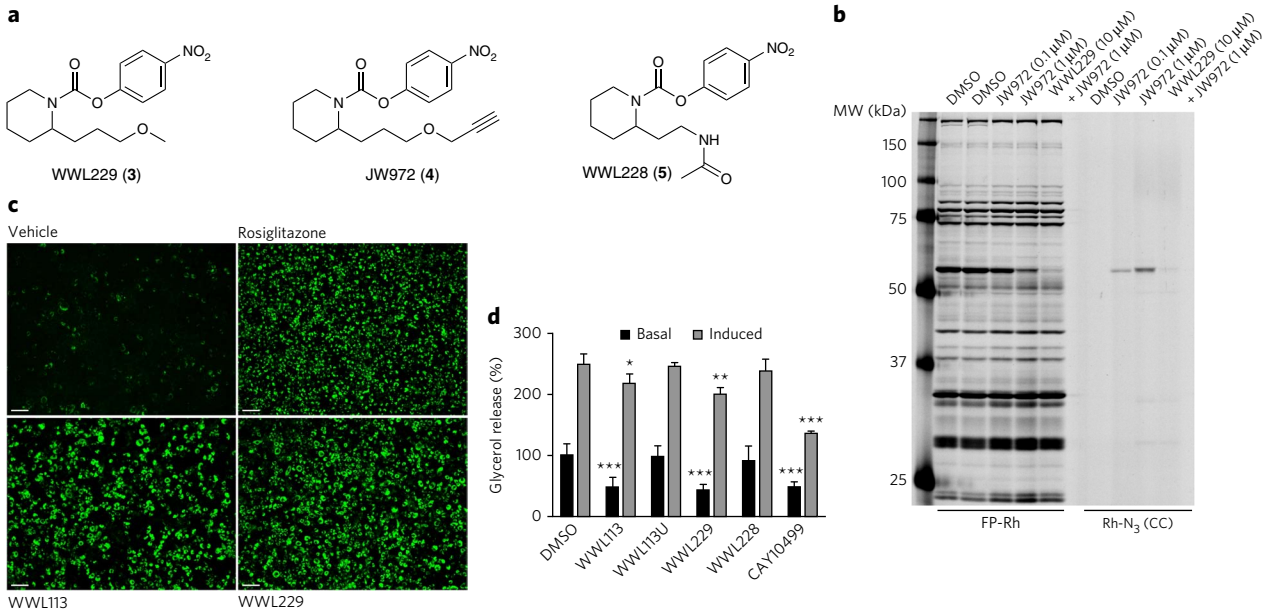

Figure 2 | WWL229, a selective Ces3 inhibitor, recapitulates the effects of WWL113 in adipocytes. (**a**) Structures of WWL229, WWL228 and JW972. (**b**) Gel-based ABPP analysis of proteomes from adipocytes incubated *in situ* for 4 h with JW972 alone or in combination with WWL229 and subsequently labeled *in vitro* with FP-rhodamine (FP-Rh) or with rhodamine-azide (Rh-N_3). The WWL229-click probe (JW972) labels an activity that is competed away by an excess of WWL229. Gel is representative of three independent experiments. MW, molecular weight; CC, click chemistry. (**c**) WWL229 (10 μM) promotes adipocyte formation and lipid storage in 10T1/2 cells to the same extent as WWL113. Green fluorescence (Nile red staining) was measured at day 8 of differentiation. Scale bars, 200 μm; images are representative of five independent experiments. (**d**) WWL229 and WWL113 block basal lipolysis in 10T1/2 adipocytes to an equivalent degree. WWL228 and WWL113U have no effect. CAY10499 is a promiscuous lipolysis inhibitor. Data are presented as mean ± s.d. ($n = 4$), $^{*}P < 0.05$, $^{**}P < 0.01$ and $^{***}P < 0.001$ in vehicle-treated cells versus treated cells.

we chose to screen a focused library of serine hydrolase inhibitors in a phenotypic screen for cellular adipogenesis and lipid storage. Serine hydrolases have important roles in many physiological and disease processes, including lipid metabolism and adipocyte function (for example, hormone sensitive lipase (HSL, also known as Lipe)) and diabetes (for example, DPPIV)[15,17]. Previous studies have inventoried serine hydrolase activities in adipocytes using phosphonate probes, but in these experiments a comparison to predifferentiated cells was not performed[18–20]. With this goal in mind, we profiled serine hydrolase activities in predifferentiated and differentiated C3H10T1/2 (10T1/2) and 3T3-L1 cells using reporter-tagged fluorophosphonates (FPs), which have been shown to serve as near-universal activity probes for mammalian serine hydrolases[21]. Proteomes from undifferentiated and differentiated 10T1/2 and 3T3-L1 cells were incubated with either a fluorescent FP probe (FP-rhodamine) to visualize serine hydrolase activity by SDS-PAGE and in-gel fluorescence scanning or with a biotinylated FP probe (FP-biotin) for affinity enrichment, identification and quantification of active serine hydrolases using avidin chromatography coupled with multidimensional liquid chromatography-MS/MS (ABPP-MudPIT)[22]. We found that adipogenesis was accompanied by the suppression of a handful of serine hydrolases that were primarily active in the predifferentiated state and by the robust induction of many other serine hydrolase activities that were elevated in mature adipocytes (**Fig. 1a** and **Supplementary Results**, **Supplementary Table 1** and **Supplementary Data Sets 1** and **2**). Serine hydrolase activities enriched in adipocytes include not only enzymes previously associated with lipid metabolism in fat cells (for example, FAS, HSL and LPL) but also many poorly annotated proteins with no prior link to adipogenesis (for example, ABHD11, ABHD6 and Serhl). The extensive induction of serine hydrolase activities during adipogenesis points to the potential importance of these enzymes in adipocyte physiology.

Screen to discern important adipocyte serine hydrolases

The existence of a large number of uncharacterized serine hydrolase activities in mature fat cells highlights the opportunity to elucidate new enzymatic pathways involved in adipose tissue biology. We sought to identify those most relevant to fat cell physiology by screening a library of serine hydrolase-directed inhibitors. Carbamates with an activated leaving group serve as a privileged scaffold for serine hydrolase inhibitors[23]. A recent *in vitro* screen of >140 carbamates against a panel of 72 serine hydrolases[21] led to the discovery of lead inhibitors for >30 serine hydrolases, underscoring the potential to identify pharmacological probes for these enzymes using a modestly sized library. We screened this carbamate library[21] in a phenotypic assay for adipocyte formation and lipid storage; compounds that score as hits in this screen can have potential as insulin sensitizers *in vivo*[13]. 10T1/2 preadipocytes were induced to differentiate into adipocytes in the presence of either vehicle (DMSO) or one of the carbamate compounds (10 μM). The PPARγ ligand rosiglitazone served as a positive control. Cells were incubated with compounds for 8 d, and the extent of adipocyte differentiation was evaluated using a fluorescent lipid dye (Nile red). This screen yielded a number of carbamates that promoted a substantial increase of lipid accumulation in differentiating adipocytes. These molecules had similar effects in 3T3-L1 cells (**Supplementary Fig. 1**).

We next used competitive ABPP to identify the molecular targets of proadipogenic carbamates. In this modality of ABPP, cells or proteomes are exposed to the bioactive carbamate before labeling with an FP probe. Serine hydrolases that react with a carbamate inhibitor are detected by a loss in their FP probe labeling. 10T1/2 adipocytes were treated for 4 h with each hit (10 μM) from the phenotypic screen, proteomes were harvested, and serine hydrolase activity was evaluated using the FP-rhodamine probe (**Fig. 1b**). Some of the carbamates (for example, WWL38) were found to target an ~80- to

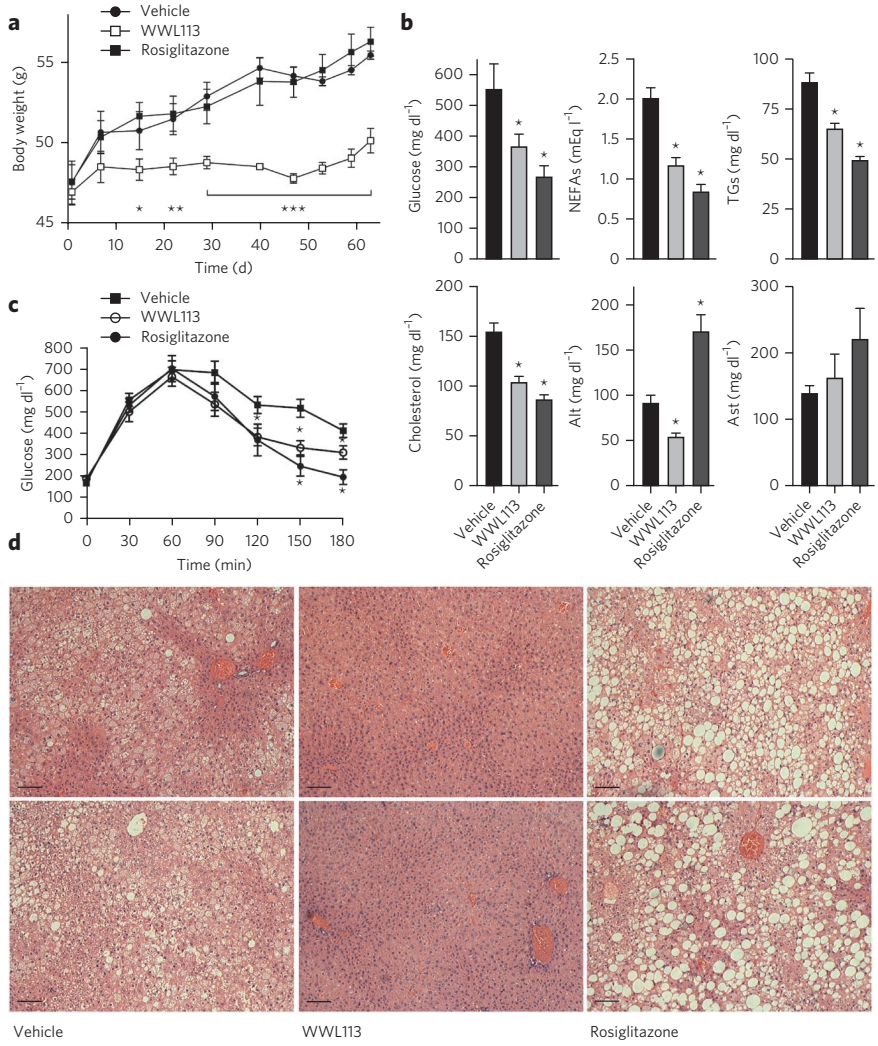

Figure 3 | WWL113 treatment corrects multiple features of metabolic syndrome in *db/db* mice. Eight-week-old *db/db* mice (n = 10 per group) were dosed orally once a day with vehicle, 30 mg per kg body weight WWL113 or 4 mg per kg body weight rosiglitazone. (**a**) WWL113-treated *db/db* mice put on weight at a slower rate. (**b**) Blood chemistry after 3 weeks of WWL113 treatment. WWL113 treatment lowers circulating glucose, NEFAs, TGs and total cholesterol. (**c**) WWL113 enhances glucose tolerance after 8 d of treatment in animals of equivalent weight. Glucose tolerance test (1 g per kg intraperitoneal injection); n = 10 per group. (**d**) Complete clearance of hepatic lipids in *db/db* mice treated with WWL113 for 3 months (hematoxylin and eosin staining showing two representative animals per group; accumulated lipids appear white). Scale bars, 100 µm. In all cases, error bars represent s.e.m. and $^*P < 0.05$, $^{**}P < 0.01$ and $^{***}P < 0.001$ versus vehicle-treated mice.

95-kDa serine hydrolase doublet that we surmised (and later confirmed by ABPP-MudPIT; **Supplementary Fig. 2a** and **Supplementary Data Set 2**) to represent HSL, an enzyme known to regulate neutral lipid catabolism in adipocytes[24]. Another set of pro-adipogenic carbamates, however, inhibited a distinct ~60-kDa serine hydrolase activity (**Fig. 1b**). We selected one of these carbamates, WWL113 (**1**) (**Fig. 1c**), which appeared to show excellent selectivity for the 60-kDa serine hydrolase (or hydrolases), for further characterization.

To gain confidence that the pro-adipogenic ability of WWL113 was due to serine hydrolase inhibition, we tested the properties of a urea analog (WWL113U (**2**); **Fig. 1c**), which should be impaired in its capacity to inhibit serine hydrolases owing to reduced reactivity. Only WWL113, and not WWL113U, showed activity in the original phenotypic assay (**Fig. 1c**). Cells treated with WWL113, and not with WWL113U, showed increased expression of fat cell markers (e.g., the transcription factors PPARγ and C/EBPα and the hormone adiponectin), indicating that they are functional adipocytes (**Supplementary Fig. 2b**). Notably, the ~60-kDa target (or targets) of WWL113 was not inhibited by WWL113U (**Fig. 1d**), confirming the utility of this agent as a negative-control probe. The putative ~60-kDa target (or targets) of WWL113 was also strongly elevated during adipocyte differentiation, with the activity being undetectable in preadipocytes and increasing steadily from day 3 to day 10 of differentiation (**Fig. 1d**). WWL113 is not a PPARγ ligand, as evaluated using transfections and a cell-free binding assay, excluding this explanation for its effect in adipocytes (**Supplementary Fig. 3**).

WWL113 is a Ces3 and Ces1f inhibitor

We next used ABPP-MudPIT to identify the target (or targets) of WWL113. The 10T1/2 adipocyte proteome was incubated with either DMSO or 10 µM WWL113 for 45 min and then treated with FP-biotin (5 µM, 2 h). Active serine hydrolases (i.e., FP-biotin labeled) were enriched using avidin beads, subjected to tryptic digestion and analyzed by ABPP-MudPIT[22]. Serine hydrolase activities were quantified by spectral counting, which revealed that WWL113 inhibited two carboxylesterase enzymes, Ces3 (also known as Ces1d) and Ces1f (also known as CesML1), with molecular weights (61,788 Da and 61,612 Da, respectively) that match the ~60-kDa activity observed by gel-based ABPP (**Fig. 1e** and **Supplementary Data Set 3**). WWL113 treatment also reduced the activity signals for ABHD6, although these data did not reach statistical significance (P = 0.08). Ces3 and Ces1f are endoplasmic reticulum glycoproteins that have been previously associated with adipocyte lipolysis[25–28]. Importantly, WWL113 did not inhibit any of the other serine hydrolases detected by ABPP-MudPIT, including several known to be involved in adipocyte lipolysis, such as HSL and monoglyceride lipase.

Acute treatment of differentiated adipocytes with WWL113, but not WWL113U, diminished basal and, to a lesser extent, hormone-induced lipolysis, suggesting a functional role for the target of this compound in the regulation of lipid breakdown in fat cells (**Supplementary Fig. 2c**). Consistent with this premise, untargeted metabolite profiling of 10T1/2 adipocytes differentiated in the presence of 10 µM WWL113 identified several elevated triacylglycerol (TAG) species (**Supplementary Fig. 4**). Some of these TAGs were also increased in cells differentiated in the presence of 1 µM rosiglitazone, whereas others, in particular long-chain, polyunsaturated TAGs, seemed to accumulate to a greater degree in WWL113-treated cells (**Supplementary Fig. 4**). None of these changes were observed in cells treated with WWL113U.

Discovery of a more selective, distinct Ces3 inhibitor

We confirmed that WWL113, but not WWL113U, is a potent inhibitor of Ces3 and Ces1f by competitive ABPP of enzymes recombinantly expressed in HEK293T cells (half-maximum inhibitory concentration (IC_{50}) value of ~0.1 µM for each enzyme; **Supplementary Fig. 5**). We also established that WWL113 inhibits recombinantly expressed ABHD6 (**Supplementary Fig. 6a**). We next

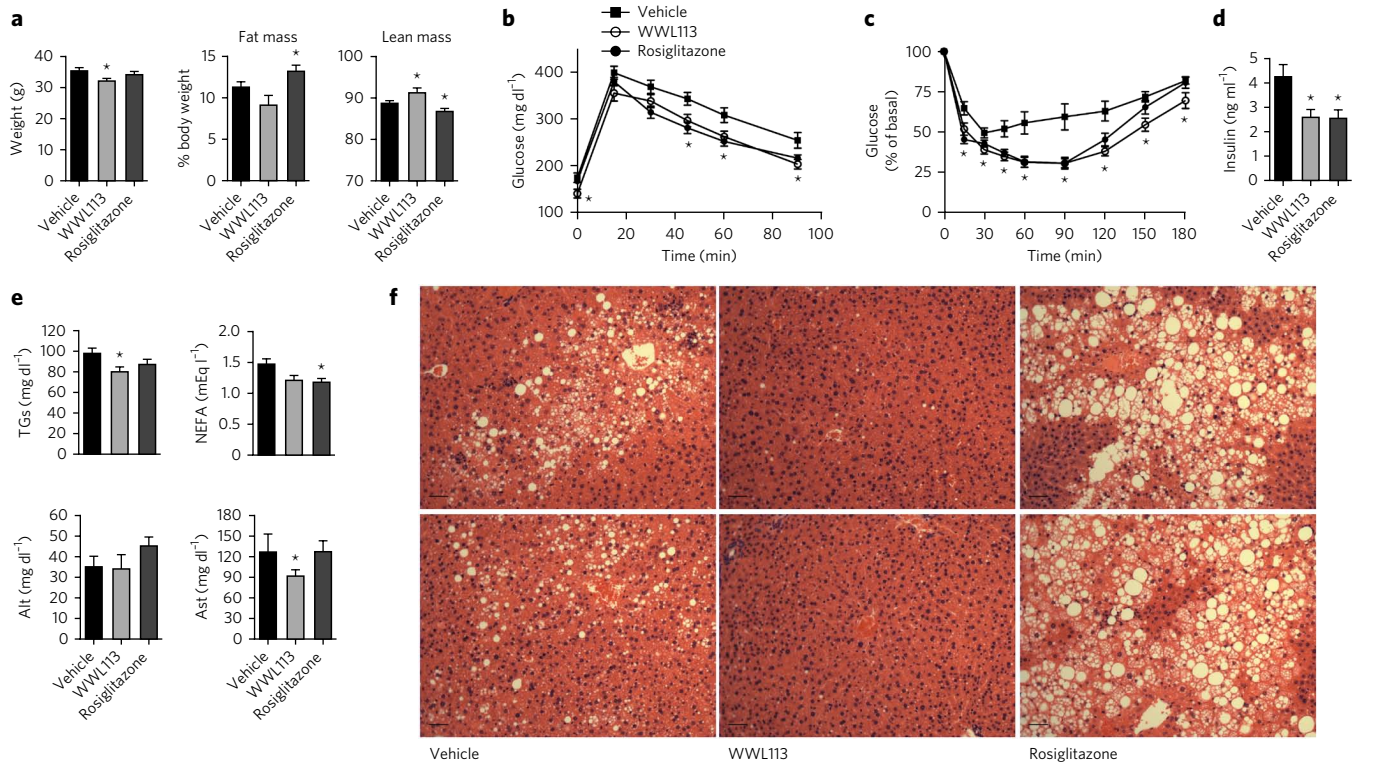

Figure 4 | WWL113 treatment enhances insulin sensitivity and glucose tolerance in a model of diet-induced obesity. 12-week-old C57BL/6J male mice fed a 60 kcal% fat diet since the time of weaning were treated orally once daily with vehicle, 50 mg per kg body weight WWL113 or 4 mg per kg body weight rosiglitazone for 50 d (n = 10 per group). (**a**) Body weight is decreased in DIO mice treated with WWL113 without a significant change in fat mass. (**b**,**c**) Glucose (**b**) and insulin (**c**) tolerance tests show that WWL113 enhances insulin sensitivity and glucose homeostasis. (**d**) WWL113 treatment decreases plasma insulin. (**e**) WWL113 treatment significantly reduces plasma triglyceride levels and shows a tendency to decrease circulating free fatty acids. The levels of aspartate aminotransferase are also significantly reduced, perhaps as a consequence of the absence of liver steatosis in WWL113-treated mice. (**f**) Hematoxylin and eosin staining showing two representative animals per group. Accumulated lipids appear white. Scale bars, 60 μm. In all cases, error bars represent s.e.m., and *P < 0.05 versus vehicle-treated mice.

used gel-based competitive ABPP to identify a second, structurally distinct carbamate (WWL229 (**3**); **Fig. 2a**) that inhibited recombinant Ces3 but not Ces1f, ABHD6 or other tested serine hydrolases (**Supplementary Fig. 6**). WWL229 also selectively inhibited Ces3 but not Ces1f, ABHD6 or other serine hydrolases in adipocyte proteomes, as determined by ABPP-MudPIT (**Supplementary Fig. 7** and **Supplementary Data Set 4**). We examined whether WWL229 reacts with other proteins in adipocyte proteomes beyond serine hydrolases by creating an alkyne-derivatized analog JW972 (**4**) (**Fig. 2a** and **Supplementary Note**), which enabled proteome-wide reactivity analysis by click chemistry–ABPP[29]. Labeling of cultured adipocytes *in situ* with JW972, followed by copper-catalyzed conjugation to an azide-rhodamine reporter tag (click chemistry[30]), revealed a single ~60-kDa protein target across the adipocyte proteome, and the labeling of this target by JW972 was substantially blocked by pretreatment with WWL229 (**Fig. 2b**). We also enriched proteins labeled by JW972 (1 μM) using an azide-biotin tag and ABPP-MudPIT methods, which identified only two JW972-labeled proteins across the entire adipocyte proteome, Ces3 and Ces1f (**Supplementary Fig. 8** and **Supplementary Data Sets 5** and **6**). We suspect that Ces1f was also enriched by JW972, even though it showed a much lower potency of inhibition compared to Ces3 (**Supplementary Fig. 5**), because only a small fraction of protein labeling may be needed to enable enrichment and identification by ABPP-MudPIT.

Notably, we found that WWL229 recapitulated all of the biological effects of WWL113 in cultured adipocytes to an equivalent extent, including the promotion of lipid storage in adipocytes (**Fig. 2c**) and the blockade of basal lipolysis (**Fig. 2d**). These effects were not observed with WWL228 (**5**), a structural analog of WWL229 that does not inhibit Ces3 activity (**Fig. 2** and **Supplementary Fig. 6**).

WWL113 treatment ameliorates obesity-diabetes in mice

One attribute of carbamate-based irreversible inhibitors of serine hydrolases, especially when used in combination with competitive ABPP, is that they provide a relatively straightforward class of probes for *in vivo* studies that often do not require extensive phamacokinetic optimization[21]. In this approach, animals are dosed with the carbamate of interest, and tissues are harvested and labeled with FP-probes to discern inhibited serine hydrolase activities at the tested dose of carbamate. Because pilot studies indicated that WWL113 exhibited markedly greater inhibitory activity in mice compared to WWL229, we chose WWL113 for *in vivo* experiments. To evaluate the potential of WWL113 as a tool compound for animal studies, mice were given a single 30 mg per kg body weight oral dose of WWL113, and tissues were analyzed 4 h later. This dose was sufficient to inhibit Ces3 activity in liver (>90%) and adipose tissue (>75%; **Supplementary Fig. 9a**), the sites of highest Ces3 expression[31]. ABPP-MudPIT revealed that the activity of several other related Ces enzymes was affected by WWL113 treatment (**Supplementary Fig. 9b**,**c** and **Supplementary Data Sets 7** and **8**). In white adipose tissue (WAT), Ces1f and esterase 22 (Ces1e), two additional Ces enzymes with lower ABPP signals than Ces3 (4- and 14-fold less, respectively), were also inhibited by WWL113. In liver, Ces1 (Ces1g), esterase1 (Ces1c) and AADAC were also inhibited by WWL113. *In vitro* assays with recombinant proteomes indicated that Ces3, Ces1f, Ces1 and Ces1c are direct targets of WWL113; changes in the activity of other hydrolases (for example, Es22) may

reflect indirect regulation of these enzymes as a result of Ces3 inhibition (**Supplementary Fig. 9d**). Because multiple CES enzymes are capable of hydrolyzing TAGs (for example, both Ces3 and Ces1f have this enzymatic activity[27,28]), we conclude that WWL113 may offer a valuable *in vivo* pharmacological probe to test the role that this group of enzymes has in obesity and type 2 diabetes.

Daily oral administration of WWL113 (30 mg per kg body weight) to obese-diabetic *db/db* mice for 9 weeks resulted in major improvement of multiple features of metabolic syndrome. Treated mice gained weight at a much slower rate than those receiving vehicle or rosiglitazone (4 mg per kg body weight), a synthetic PPARγ ligand used as a control for enhanced insulin sensitivity (**Fig. 3a**). This effect was noted within 2 weeks of WWL113 administration and could not be ascribed to decreased food intake or intestinal lipid absorption (**Supplementary Fig. 10a**,**b**). Plasma analysis after 3 weeks of treatment showed marked improvement in glucose and lipid profiles comparable to that brought about by the clinical agent rosiglitazone (**Fig. 3b**). Mice treated with WWL113 had lower levels of nonesterified free fatty acids (NEFAs), triglycerides (TGs), total cholesterol and fasted glucose as well as enhanced glucose tolerance (data not shown). To examine the possibility that improved glucose tolerance in WWL113-treated mice was due to their reduced weight, a second set of *db/db* mice was treated with WWL113, and the test was performed after 8 d of dosing, a point at which there were no weight differences between groups (**Supplementary Fig. 10c**). Glucose tolerance was enhanced in diabetic mice treated with WWL113 in this short regimen (**Fig. 3c**).

Much of the beneficial impact that WWL113 treatment had on metabolic parameters may have been due to its marked effect on hepatic lipid accumulation. Ectopic fat deposition in the liver is a common feature of obesity and type 2 diabetes that may render this organ less sensitive to insulin[32]. In stark contrast to animals treated with the PPARγ ligand, which showed increased liver lipid accumulation (a side effect of thiazolidinediones in rodents[33]), obese-diabetic mice treated chronically with WWL113 displayed complete clearance of the excess lipids that normally accrue in the liver of these animals (**Fig. 3d**). Resolution of hepatic steatosis was accompanied by unchanged aspartate aminotransferase (Ast) and decreased alanine aminotransferase (Alt) activity, markers of liver damage (**Fig. 3b**). Expression of liver lipogenic genes (for example, *Srebf1*) was decreased in WWL113-treated animals, whereas expression of genes involved in fatty acid oxidation and ketogenesis was induced (for example, *Ppara*, *Acadl* and *Hmgcl*) (**Supplementary Fig. 10d**). These changes were reflected in an increase in circulating ketone bodies, the end product of fatty acid oxidation, that became evident within 2 weeks of the start of WWL113 treatment (**Supplementary Fig. 10e**). These increases in oxidative gene expression were not due to direct activation of PPARα by WWL113 (**Supplementary Fig. 3a**). Wild-type mice treated for 30 d with the same dose of WWL113 showed no difference in weight or glycemia, indicating that the changes WWL113 elicited in diabetic mice are not due to toxic effects (**Supplementary Fig. 11**).

Treatment with WWL113 had similar effects in diet-induced obesity (DIO) mice, a nongenetic model that more closely resembles the development of obesity and insulin resistance in humans. C57BL/6J mice were fed a high-fat diet for 12 weeks before the start of 9 weeks of compound treatment (oral 50 mg per kg body weight daily dose). DIO mice dosed with WWL113 were more resistant to weight gain than controls and showed enhanced glucose tolerance (**Fig. 4a**,**b**). WWL113-treated mice also had lower levels of plasma insulin and increased whole-body insulin sensitivity, as measured using insulin tolerance tests (**Fig. 4c**,**d**). Circulating triglycerides were significantly ($P = 0.02$) decreased, whereas NEFAs showed a downward trend that did not reach statistical significance (**Fig. 4e**). Although white adipocytes in the visceral and subcutaneous depots of WWL113-treated mice seemed larger than those in vehicle-treated animals, this difference was not considerable. The changes seen in the liver were more notable. WWL113-treated animals showed complete absence of ectopic lipid deposition in the liver (**Fig. 4f**). Together, these data indicate that inhibition of Ces3 and Ces1f activity has multiple beneficial effects in lipid and glucose homeostasis in genetic and diet-induced mouse models of obesity, insulin resistance and type 2 diabetes.

Table 1 | Hepatic lipid levels in WWL113-treated mice.

	db/db, 14 d	WT, 4 h
MAGs		
C16:0 MAG	0.6	0.8
C18:0 MAG	0.4*	1.5
C20:4 MAG	0.7*	0.5*
DAGs		
C32:0 DAG	0.7**	0.9
C34:2 DAG	0.4**	0.8
C34:1 DAG	0.2**	0.9
C36:4 DAG (C16:0/C20:4 DAG)	0.3**	0.5**
C38:5 DAG (C18:1/C20:4 DAG)	0.6**	0.6*
TAGs		
C48:2 TAG	0.4**	1.0
C50:2 TAG	0.4**	1.2
C52:4 TAG	0.7*	1.7
C52:3 TAG	0.7	1.2
C52:1 TAG	0.6*	1.1
C54:5 TAG	0.6**	1.0
C52:4 TAG	0.5**	0.9
C54:3 TAG	0.5**	0.9
C56:6 TAG	0.7	0.9
LPC		
C16:0 LPC	0.9	1.2
PC		
C34:1 PC	0.8	1.2
C36:1 PC	0.9	1.1
Acylcarnitine		
C16:0 acylcarnitine	1.2	0.9

Values shown represent WWL113/control. LPC, lysophosphatidylcholine; PC, phosphatidylcholine. *$P < 0.05$, **$P < 0.01$ with >1.4-fold or <0.7-fold of control. '*db/db* 14 d' refers to *db/db* mice treated chronically with WWL113. 'WT, 4h' refers to wild-type mice treated acutely with a single dose of WWL113 and analyzed 4 h later.

WWL113 treatment reduces hepatic diacylglycerol species

The marked effects of WWL113 treatment on liver lipid accumulation prompted us to explore the nature of the metabolite changes induced by this compound. Livers from *db/db* mice treated with WWL113 for 14 d were subjected to lipidomic analysis. Consistent with the histology, lipid profiling revealed that various TAG, diacylglycerol (DAG) and monoacylglycerol (MAG) species were significantly reduced in mice dosed with WWL113 (**Table 1**). Changes were not observed in the levels of other detected lipid species, such as phospholipids. To discern which of these changes were directly related to Ces3 and Ces1f inhibition, as opposed to those which were a consequence of the enhanced metabolic state of treated animals, wild-type mice were given a single dose of WWL113, and their livers were analyzed 4 h later. In this acute setting, the levels of bulk TAG species did not change, but those of several DAG and MAG

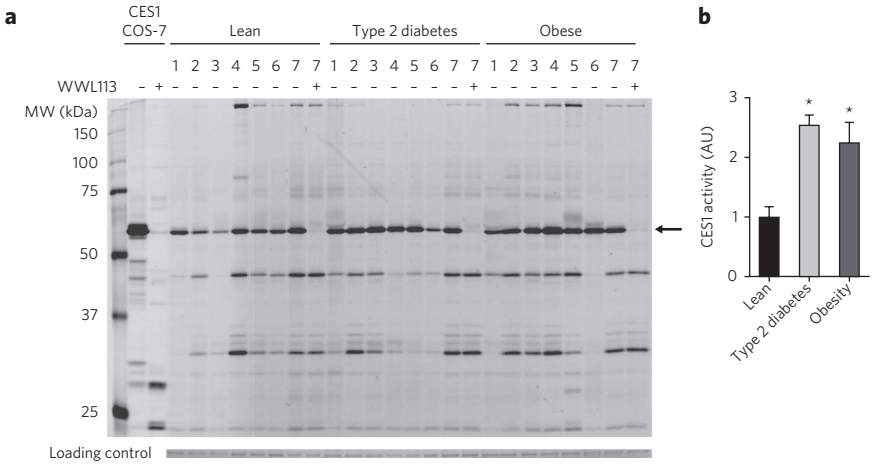

Figure 5 | hCES1 is more active in adipose tissue of obese and type 2 diabetic individuals. (**a**) ABPP profiles of WAT samples from seven lean, obese and type 2 diabetic individuals. hCES1 (black arrow) is detected, and WWL113 (10 uM) inhibits this human homolog of Ces3. The leftmost two lanes are lysates of COS-7 cells ectopically expressing hCES1. (**b**) Bar graph shows quantification of hCES1 activity relative to a Coomassie-stained band that is similarly abundant in all of the samples (loading control). Error bars represent s.e.m. and $^*P < 0.05$ versus lean controls.

species, including 16:0/20:4 DAG and 20:4 MAG, were significantly decreased (**Table 1**). These findings are consistent with the proposed role of Ces3 and Ces1f as endoplasmic reticulum–localized triacylglycerol hydrolases that act on limited TAG pools[31].

hCES1 is more active in obesity and diabetes

To explore the extent to which our findings in rodents may translate to humans, we measured the activity of hCES1 (the ortholog of mouse Ces3) by gel-based ABPP in adipose tissue biopsies of lean (body mass index (BMI) < 25), obese (BMI 31.8–55.8, mean 37.2; mean hemoglobin A1c (Hb A1c) 4.9) and type 2 diabetic (BMI 32.7–61, mean 41.7; Hb A1c 6.7–11.2, mean 8.7) individuals. Similar to what we observed with Ces3 in mice, we found hCES1 was a highly active serine hydrolase in white fat. Though there was heterogeneity among human samples, the levels of hCES1 activity were increased roughly twofold in obese individuals and patients with type 2 diabetes compared to lean subjects (**Fig. 5**). Enhanced hCES1 activity and the consequent release of greater numbers of fatty acids into the circulation may be a heretofore unrecognized feature of the pathogenesis of obesity-diabetes. Notably, WWL113 also inhibited hCES1, as assessed using gel-based ABPP (**Fig. 5a**) and a substrate hydrolysis assay (**Supplementary Fig. 12**; IC_{50} ~50 nM).

DISCUSSION

Renewed interest in phenotypic screens for drug discovery is being driven by advances in chemical proteomics that are enabling identification of the molecular targets of bioactive compounds. Common chemical proteomic strategies for target identification involve generating affinity matrices or photoreactive derivatives of the bioactive small molecule[4]. MS-based proteomics of enriched proteins then provides a list of likely targets, and molecular biology (for example, RNAi) or other means are used to confirm the target (or targets) responsible for the observed biological effect. Although productive, these approaches require derivatization of screening hits, which can impair target interactions. Even in cases where target identification is successful, considerable medicinal chemistry is often required to convert screening hits into probes that can be used for biological studies.

Here, we employed an alternative approach based on phenotypic screening of a focused small-molecule library of carbamates designed to inhibit a specific enzyme class (serine hydrolases), followed by competitive ABPP to identify the protein targets of bioactive hits. The special features of carbamates, which include drug-like structures and an irreversible mechanism of inhibition, facilitate swift *in vivo* validation of new targets without requiring extensive medicinal chemistry optimization. Our phenotypic assay selected molecules that promote adipocyte differentiation and lipid storage in fat cells. The notion that molecules that induce fat cell formation would be beneficial in diabetes may seem counterintuitive, given the association between obesity and the development of insulin resistance and diabetes. However, obesity-linked insulin resistance is associated with increased levels of circulating free fatty acids and ectopic lipid deposition[14]. In obesity, the hypertrophied adipocyte is not able to properly store excess fatty acids, and, as a result, these lipids deposit in other tissues where they hinder insulin action[34]. Compounds that can restore normal lipid partitioning among tissues and potentiate adipocyte function (for example, TZDs) may thus enhance systemic insulin action. Several adipogenic carbamates from our screen inhibited the same target, a ~60-kDa serine hydrolase that was identified by competitive ABPP-MudPIT as Ces3 (also known as Ces1d or TGH).

Ces3 has been shown through genetic methods to be involved in lipolysis[27], the process whereby the adipocyte hydrolyzes stored triglycerides into fatty acids to be used as fuel by other tissues in times of need. Hormonally induced lipolysis is controlled by catecholamines and insulin and is mediated by other serine hydrolases (ATGL (also known as desnutrin), HSL and MGLL)[24]. In contrast, Ces3 has been reported to be important for basal lipolysis[27], in agreement with our observation that WWL113 and WWL229 block this process. Increased adipocyte lipolysis is a central feature of insulin resistance and type 2 diabetes[32,34]: it generates surplus fatty acids that deposit ectopically in tissues and excess glycerol that the liver uses to boost glucose production. Compounds that inhibit lipolysis can improve insulin sensitivity in type 2 diabetes patients[35,36]. Strategies to target obesity-linked increases in lipolysis have focused on inhibition of hormone-induced lipolysis, a process that is part of the normal response to fasting and feeding. Animal models have questioned the wisdom of systemic blockade of hormone-induced lipolysis[37], and these drug discovery efforts have yet to translate into clinical agents. Here, we have shown that pharmacologic restrain of basal lipolysis (via Ces3 inhibition) is sufficient to elicit therapeutic benefits *in vivo*. Because Ces3 and hCES1 inhibitors will block primarily basal lipolysis, they may prove safer than molecules that hamper hormone-induced lipolysis.

Treatment with WWL113 ameliorated multiple features of metabolic syndrome in models of genetic and diet-induced obesity and insulin resistance and diabetes. The compound acts primarily at the two tissues of greatest Ces3 activity, adipose and liver. In fat, Ces3 inhibition blocks basal lipolysis and enhances adipocyte function. In liver, WWL113 treatment decreases expression of lipogenic genes while simultaneously increasing expression of fatty acid oxidation and ketogenesis enzymes. These changes, most likely coupled to reduced fatty acid and glycerol efflux from adipocytes, prevent steatosis and enhance liver insulin sensitivity. Ces3 has been shown to be important for hydrolysis of hepatic TG stores before reesterification and assembly into apoB-containing very low-density lipoprotein (VLDL)-TG particles[31]. Inhibition of Ces3 in rat primary hepatocytes decreases VLDL secretion, which may appear at odds with the lack of lipid accumulation in the liver of WWL113-treated mice[38]. However, Ces3-null primary hepatocytes show increased

fatty acid oxidation[39]. Thus, the phenotype we observe in treated mice most likely reflects the balance of decreased synthesis and increased oxidation of hepatic fatty acids and reduced influx of adipocyte-derived fatty acids.

Contrary to the profile of WWL113 in cultured adipocytes, competitive ABPP-MudPIT of tissues revealed that this compound also inhibits the closely related carboxylesterases Ces1f, Ces1 and Ces1c *in vivo*. Although we cannot exclude the possibility that these poorly characterized enzymes might contribute to the effects of WWL113, we should mention that all of the major effects of WWL113 treatment are recapitulated by genetic ablation of Ces3 (ref. 39). Mice lacking Ces3 fed a standard diet show decreased plasma triglycerides and free fatty acids, lack of liver steatosis, enhanced insulin sensitivity and glucose tolerance, augmented hepatic fatty acid oxidation and increased energy expenditure (which may explain the resistance to weight gain in WWL113-treated mice, though we have no direct evidence of this). In contrast, Ces1-null mice develop obesity, hyperlipidemia, fatty liver, hyperinsulinemia and insulin resistance on a normal diet[40]. Moreover, consistent with the effect of WWL113 in cultured adipocytes, RNAi studies have shown that Ces3 knockdown blocks basal lipolysis without a major effect on hormone-induced lipolysis[27]. Finally, we have shown that a second structurally unrelated carbamate that shows complete Ces3 selectivity (WWL229) recapitulates all of the effects seen with WWL113 in adipocytes. Thus, we believe that our set of Ces3-directed chemical probes has provided pharmacological evidence supporting the utility of Ces3 inhibition in models of obesity-diabetes. It is interesting to note that recently described liver-specific Ces3-null mice have decreased cholesterol and triglycerides in plasma but moderately increased levels in liver[41]. More importantly, these mice do not show enhanced glucose tolerance, and females display decreased insulin sensitivity. These findings suggest that adipose tissue may be a primary determinant of the benefits we have observed upon pharmacologic inhibition of Ces3.

The carboxylesterase family is considerably more complex in mice than humans, and many mouse enzymes lack human orthologs (for example, Ces1f and Ces1c)[42]. In humans, hCES1 has been studied primarily as a liver detoxification enzyme[43]. However, increased hCES1 mRNA in adipose tissue has been associated with obesity and metabolic impairments in obesity-discordant sibling studies[44] and in several other human populations[45–47]. Our data indicate that hCES1 activity is increased in WAT of obese and type 2 diabetics. Hence, hCES1 inhibition in humans may produce similar metabolic benefits as are seen in mice treated with a Ces3 inhibitor.

We have outlined an approach integrating phenotypic screening with ABPP that can simplify the process of target identification and *in vivo* validation of screening results. Broad-spectrum activity-based probes have been developed for multiple enzyme classes beyond serine hydrolases[48–50]. In principle, our approach should be applicable to evaluate the function of other enzyme classes in any desired biological output that can be reduced to a cell-based assay. Our work has also uncovered multiple poorly annotated serine hydrolases active during adipogenesis, underscoring the potential of ABPP to contribute to the discovery of biochemical pathways that support complex cellular processes.

Received 25 June 2013; accepted 21 November 2013;
published online 22 December 2013

METHODS

Methods and any associated references are available in the online version of the paper.

References

1. Kodadek, T. Rethinking screening. *Nat. Chem. Biol.* **6**, 162–165 (2010).
2. Swinney, D.C. & Anthony, J. How were new medicines discovered? *Nat. Rev. Drug Discov.* **10**, 507–519 (2011).
3. Hahn, C.K. *et al.* Proteomic and genetic approaches identify Syk as an AML target. *Cancer Cell* **16**, 281–294 (2009).
4. Rix, U. & Superti-Furga, G. Target profiling of small molecules by chemical proteomics. *Nat. Chem. Biol.* **5**, 616–624 (2009).
5. Moellering, R.E. & Cravatt, B.F. How chemoproteomics can enable drug discovery and development. *Chem. Biol.* **19**, 11–22 (2012).
6. Laggner, C. *et al.* Chemical informatics and target identification in a zebrafish phenotypic screen. *Nat. Chem. Biol.* **8**, 144–146 (2012).
7. Wacker, S.A., Houghtaling, B.R., Elemento, O. & Kapoor, T.M. Using transcriptome sequencing to identify mechanisms of drug action and resistance. *Nat. Chem. Biol.* **8**, 235–237 (2012).
8. Ong, S.E. *et al.* Identifying the proteins to which small-molecule probes and drugs bind in cells. *Proc. Natl. Acad. Sci. USA* **106**, 4617–4622 (2009).
9. Raj, L. *et al.* Selective killing of cancer cells by a small molecule targeting the stress response to ROS. *Nature* **475**, 231–234 (2011).
10. Cravatt, B.F., Wright, A.T. & Kozarich, J.W. Activity-based protein profiling: from enzyme chemistry to proteomic chemistry. *Annu. Rev. Biochem.* **77**, 383–414 (2008).
11. Heal, W.P., Dang, T.H. & Tate, E.W. Activity-based probes: discovering new biology and new drug targets. *Chem. Soc. Rev.* **40**, 246–257 (2011).
12. Leung, D., Hardouin, C., Boger, D.L. & Cravatt, B.F. Discovering potent and selective reversible inhibitors of enzymes in complex proteomes. *Nat. Biotechnol.* **21**, 687–691 (2003).
13. Waki, H. *et al.* The small molecule harmine is an antidiabetic cell-type–specific regulator of PPARγ expression. *Cell Metab.* **5**, 357–370 (2007).
14. McGarry, J.D. Banting lecture 2001: dysregulation of fatty acid metabolism in the etiology of type 2 diabetes. *Diabetes* **51**, 7–18 (2002).
15. Bachovchin, D.A. & Cravatt, B.F. The pharmacological landscape and therapeutic potential of serine hydrolases. *Nat. Rev. Drug Discov.* **11**, 52–68 (2012).
16. Long, J.Z. & Cravatt, B.F. The metabolic serine hydrolases and their functions in mammalian physiology and disease. *Chem. Rev.* **111**, 6022–6063 (2011).
17. Wani, J.H., John-Kalarickal, J. & Fonseca, V.A. Dipeptidyl peptidase-4 as a new target of action for type 2 diabetes mellitus: a systematic review. *Cardiol. Clin.* **26**, 639–648 (2008).
18. Morak, M. *et al.* Differential activity-based gel electrophoresis for comparative analysis of lipolytic and esterolytic activities. *J. Lipid Res.* **50**, 1281–1292 (2009).
19. Schicher, M. *et al.* Functional proteomic analysis of lipases and esterases in cultured human adipocytes. *J. Proteome Res.* **9**, 6334–6344 (2010).
20. Birner-Gruenberger, R. *et al.* Functional fat body proteomics and gene targeting reveal *in vivo* functions of *Drosophila melanogaster* α-esterase-7. *Insect Biochem. Mol. Biol.* **42**, 220–229 (2012).
21. Bachovchin, D.A. *et al.* Superfamily-wide portrait of serine hydrolase inhibition achieved by library-versus-library screening. *Proc. Natl. Acad. Sci. USA* **107**, 20941–20946 (2010).
22. Jessani, N. *et al.* A streamlined platform for high-content functional proteomics of primary human specimens. *Nat. Methods* **2**, 691–697 (2005).
23. Li, W., Blankman, J.L. & Cravatt, B.F. A functional proteomic strategy to discover inhibitors for uncharacterized hydrolases. *J. Am. Chem. Soc.* **129**, 9594–9595 (2007).
24. Zechner, R. *et al.* FAT SIGNALS—lipases and lipolysis in lipid metabolism and signaling. *Cell Metab.* **15**, 279–291 (2012).
25. Lehner, R. & Vance, D.E. Cloning and expression of a cDNA encoding a hepatic microsomal lipase that mobilizes stored triacylglycerol. *Biochem. J.* **343**, 1–10 (1999).
26. Soni, K.G. *et al.* Carboxylesterase 3 (EC 3.1.1.1) is a major adipocyte lipase. *J. Biol. Chem.* **279**, 40683–40689 (2004).
27. Wei, E., Gao, W. & Lehner, R. Attenuation of adipocyte triacylglycerol hydrolase activity decreases basal fatty acid efflux. *J. Biol. Chem.* **282**, 8027–8035 (2007).
28. Okazaki, H. *et al.* Identification of a novel member of the carboxylesterase family that hydrolyzes triacylglycerol: a potential role in adipocyte lipolysis. *Diabetes* **55**, 2091–2097 (2006).
29. Speers, A.E., Adam, G.C. & Cravatt, B.F. Activity-based protein profiling *in vivo* using a copper(i)-catalyzed azide-alkyne [3 + 2] cycloaddition. *J. Am. Chem. Soc.* **125**, 4686–4687 (2003).
30. Rostovtsev, V.V., Green, L.G., Fokin, V.V. & Sharpless, K.B. A stepwise huisgen cycloaddition process: copper(i)-catalyzed regioselective 'ligation' of azides and terminal alkynes. *Angew. Chem. Int. Edn Engl.* **41**, 2596–2599 (2002).
31. Quiroga, A.D. & Lehner, R. Role of endoplasmic reticulum neutral lipid hydrolases. *Trends Endocrinol. Metab.* **22**, 218–225 (2011).
32. Samuel, V.T. & Shulman, G.I. Mechanisms for insulin resistance: common threads and missing links. *Cell* **148**, 852–871 (2012).
33. Boelsterli, U.A. & Bedoucha, M. Toxicological consequences of altered peroxisome proliferator-activated receptor γ (PPARγ) expression in the liver: insights from models of obesity and type 2 diabetes. *Biochem. Pharmacol.* **63**, 1–10 (2002).

34. Cusi, K. The role of adipose tissue and lipotoxicity in the pathogenesis of type 2 diabetes. *Curr. Diab. Rep.* **10**, 306–315 (2010).
35. Bajaj, M. *et al.* Sustained reduction in plasma free fatty acid concentration improves insulin action without altering plasma adipocytokine levels in subjects with strong family history of type 2 diabetes. *J. Clin. Endocrinol. Metab.* **89**, 4649–4655 (2004).
36. Fulcher, G.R., Walker, M., Catalano, C., Agius, L. & Alberti, K.G. Metabolic effects of suppression of nonesterified fatty acid levels with acipimox in obese NIDDM subjects. *Diabetes* **41**, 1400–1408 (1992).
37. Girousse, A. & Langin, D. Adipocyte lipases and lipid droplet–associated proteins: insight from transgenic mouse models. *Int. J. Obes. (Lond.)* **36**, 581–594 (2012).
38. Gilham, D. *et al.* Inhibitors of hepatic microsomal triacylglycerol hydrolase decrease very low density lipoprotein secretion. *FASEB J.* **17**, 1685–1687 (2003).
39. Wei, E. *et al.* Loss of TGH/Ces3 in mice decreases blood lipids, improves glucose tolerance, and increases energy expenditure. *Cell Metab.* **11**, 183–193 (2010).
40. Quiroga, A.D. *et al.* Deficiency of carboxylesterase 1/esterase-x results in obesity, hepatic steatosis, and hyperlipidemia. *Hepatology* **56**, 2188–2198 (2012).
41. Lian, J. *et al.* Liver specific inactivation of carboxylesterase 3/triacylglycerol hydrolase decreases blood lipids without causing severe steatosis in mice. *Hepatology* **56**, 2154–2162 (2012).
42. Holmes, R.S. *et al.* Recommended nomenclature for five mammalian carboxylesterase gene families: human, mouse, and rat genes and proteins. *Mamm. Genome* **21**, 427–441 (2010).
43. Satoh, T. & Hosokawa, M. The mammalian carboxylesterases: from molecules to functions. *Annu. Rev. Pharmacol. Toxicol.* **38**, 257–288 (1998).
44. Jernås, M. *et al.* Regulation of carboxylesterase 1 (CES1) in human adipose tissue. *Biochem. Biophys. Res. Commun.* **383**, 63–67 (2009).
45. Steinberg, G.R., Kemp, B.E. & Watt, M.J. Adipocyte triglyceride lipase expression in human obesity. *Am. J. Physiol. Endocrinol. Metab.* **293**, E958–E964 (2007).
46. Nagashima, S. *et al.* Depot-specific expression of lipolytic genes in human adipose tissues–association among CES1 expression, triglyceride lipase activity and adiposity. *J. Atheroscler. Thromb.* **18**, 190–199 (2011).
47. Marrades, M.P., Gonzalez-Muniesa, P., Martinez, J.A. & Moreno-Aliaga, M.J. A dysregulation in *CES1*, *APOE* and other lipid metabolism-related genes is associated to cardiovascular risk factors linked to obesity. *Obes. Facts* **3**, 312–318 (2010).
48. Evans, M.J. & Cravatt, B.F. Mechanism-based profiling of enzyme families. *Chem. Rev.* **106**, 3279–3301 (2006).
49. Schmidinger, H., Hermetter, A. & Birner-Gruenberger, R. Activity-based proteomics: enzymatic activity profiling in complex proteomes. *Amino Acids* **30**, 333–350 (2006).
50. Edgington, L.E., Verdoes, M. & Bogyo, M. Functional imaging of proteases: recent advances in the design and application of substrate-based and activity-based probes. *Curr. Opin. Chem. Biol.* **15**, 798–805 (2011).

Acknowledgments

We thank N. Kralli and P. Tontonoz for valuable discussions. E.S. is supported by a Career Development Award from the American Diabetes Association, the McDonald's Center for Type 2 Diabetes and Obesity and US National Institutes of Health grants DK081003 and DK099810. B.F.C. is supported by NIH grant DK099810. M.J.W. is supported by grants and a Senior Research Fellowship from the National Health and Medical Research Council of Australia. A.P.R. is supported by a Career Development Fellowship from the National Health and Medical Research Council of Australia. E.D. was supported by an Anxeles Alvariño fellowship from the Xunta de Galicia, Spain. K.-L.H. was supported by a Hewitt Foundation postdoctoral fellowship.

Author contributions

E.S., E.D. and B.F.C. designed experiments. E.S., E.D., J.P., C.G. and A.G. performed cell-based, biochemical and *in vivo* experiments. W.L. and J.W.C. synthesized compounds. J.T. and D.K.N. performed lipidomic analysis. A.G., E.D. and K.-L.H. performed proteomic experiments. D.P. provided technical help. A.P.R., M.J.W. and P.E.O. provided human samples. E.D., J.P., C.G., A.G., J.T., D.K.N., K.-L. H., S.N., B.F.C. and E.S. analyzed data. E.D., B.F.C. and E.S. wrote the manuscript.

Competing financial interests

The authors declare competing financial interests: details accompany the online version of the paper.

Additional information

Supplementary information, chemical compound information and chemical probe information is available in the online version of the paper. Reprints and permissions information is available online at http://www.nature.com/reprints/index.html. Correspondence and requests for materials should be addressed to E.S.

ONLINE METHODS

Cell culture and phenotypic screen. 10T1/2 cells (ATCC) were maintained in DMEM with 10% FBS (FBS). 3T3-L1 preadipocytes (ATCC) were maintained in DMEM supplemented with 10% bovine calf serum. To induce differentiation, confluent cells were cultured in DMEM with 10% FBS and exposed to dexamethasone (1 μM; Sigma), 3-isobutyl-1-methylxanthine (0.5 mM; Sigma) and insulin (5 μg/ml; Sigma) for 3 d, followed by culture with insulin alone (5 μg/ml). In the phenotypic screen, 10T1/2 pre-adipocytes were induced to differentiate at confluence in the presence of 10 μM of each serine hydrolase inhibitor. Rosiglitazone (1 μM; Cayman) was used as a positive control. Medium was replaced every 2 d, and compounds were refreshed. On day 8 of differentiation, cells were stained with the fluorescent lipid stain Nile red (AdipoRed; Lonza), and compounds inducing increased lipid accumulation (i.e., fluorescence) were identified. Primary hits were confirmed using traditional Oil Red O staining in six-well-plate format.

Gene expression analysis. Total RNA was extracted using the NucleoSpin 96 RNA kit (Macherey-Nagel) and analyzed by TaqMan-based qRT-PCR using a one-step reagent (SuperScript III Platinum; Life Technologies). Analysis was performed on a 7900HT instrument (ABI) using the standard curve method. Samples were run in triplicate as multiplexed reactions and normalized to an internal control (*36B4*). Details of probe and primer mixes are shown below.

Gene	ABI Gene Expression Assay
Pparg	Mm00440945_m1
Adipoq	Mm00456425_m1
Cebpa	Mm00514283_s1
Lpl	Mm00434764_m1
Fas	Mm00662319_m1
Scd1	Mm00772290_m1
Mlxipl	Mm02342723_m1
Acaca	Mm01304257_m1
Ppara	Mm00440939_m1
Acadvl	Mm00444296_m1
Acadl	Mm00599660_m1
Acadm	Mm00431611_m1
Acads	Mm00431617_m1
Cpt1a	Mm00550438_m1
Hmgcs2	Mm00550050_m1
Hmgcl	Mm00468667_m1

Srebf1	Sequence
Forward primer	AGGACCCAAGGTGACACCTG
Reverse primer	GGACACGGACGGGTACATCT
Probe	CTCCACCATCGGCACCCGCT
36B4	
Reverse primer	GTTCTTGCCCATCAGCACC
Forward primer	AGATGCAGCAGATCCGCAT
Probe	CGCTCCGAGGGAAGGCCG

Fluorescence-resonance energy transfer assay. His-tagged recombinant ligand-binding domain (LBD) PPARγ protein was prepared in bacteria. Protein purity was evaluated by SDS-PAGE, and functional activity was verified using a 12-point dose response to rosiglitazone starting at 10 μM. FRET assay was performed in black flat-bottom 384-well plates in a 20-μl final volume. A mix of 20 nM His-PPARγ-LBD protein, 500 nM biotinylated SRC-1 peptide (biotin-CPSSHSSLTERHKILHRLLQEGSPSC-OH; Biopeptide), 1 nM Europium-labeled anti-His antibody (PerkinElmer; catalog no. AD0110) and 100 nM allophycocyanin-labeled streptavidin (Prozyme) was prepared in assay buffer (50 mM KCl, 50 mM Tris, pH 7.5, 0.1 mg/ml fatty acid-free bovine serum albumin and 1 mM dithiothreitol). Carbamates were tested at a final concentration of 10 μM. Plates were incubated for 1 h at RT, and FRET was read on a Pherastar (BMG Labtech).

Lipolysis assay. To measure basal lipolysis, differentiated 10T1/2 adipocytes were incubated with compounds (10 μM) for 24 h in serum-free DMEM containing 1% bovine serum albumin. For hormone-induced lipolysis, cells treated as above were stimulated with 1 μM isoproterenol (Sigma) for 1 h before collection of conditioned medium. Glycerol release into the medium was measured using a free glycerol determination kit (Sigma). CAY10499 (2 μM; a promiscuous lipolysis inhibitor) was purchased from Cayman.

ABPP of cells and tissues. To prepare proteomes for ABPP, cells were washed with PBS, collected by scraping and sonicated. Mouse tissues were Dounce-homogenized in PBS, pH 7, followed by low-speed centrifugation (1,400*g*, 3 min) to remove debris and, in the case of adipose tissue, also the fat cake. Protein concentration was determined using Lowry's method, and samples were frozen until use. For gel-based ABPP experiments, proteomes were diluted to 1 mg/ml in PBS and incubated with a rhodamine-tagged fluorophosphonate (FP-rhodamine) at a final concentration of 1 μM in a 50-μl reaction volume. Reactions were quenched after 45 min at room temperature with one volume of standard 2× SDS-PAGE loading buffer (reducing), heated at 90 °C for 8 min, separated by SDS-PAGE (10% acrylamide) and visualized in-gel using a flatbed fluorescence scanner (Hitachi FMBio IIe, MiraiBio). For competitive ABPP analysis, proteomes were preincubated with carbamates (1 μM to 50 μM) for 45 min at room temperature before the addition of the FP-rhodamine probe. FP-rhodamine was synthesized in house[51].

MudPIT analysis of ABPP samples. Proteomes from cells and tissues (for example, livers of mice treated with a single dose of WWL113) generated as described above were adjusted to a final concentration of 1 mg/ml, and 1 mg of proteome was labeled with 5 μM of FP-biotin (synthesized in house[52]) for 2 h at room temperature. After labeling, the insoluble proteome was solubilized by incubation with 1% Triton-X with agitation at 4 °C for 1 h. FP-labeled proteins in the soluble and insoluble fractions were enriched using 50 μl of avidin beads (Sigma), as described in ref. 53. The avidin-enriched proteome was sequentially washed twice for 8 min with (i) 1% SDS, (ii) 6 M urea and (iii) 50 mM Tris, pH 8.0, and finally resuspended in 150 μl 8 M urea/50 mM Tris, pH 8.0. Samples were prepared for on-bead digestion by reduction with 10 mM TCEP for 30 min at room temperature and alkylated with 12.5 mM of iodoacetamide for 30 min at room temperature in the dark. Digestions were performed for 12 h at 37 °C by addition of 3 μl of 0.5 mg/μl trypsin (Promega) in the presence of 2 mM $CaCl_2$ after samples were diluted to 2 M urea with 50 mM Tris, pH 8.0. Finally, peptide samples were acidified to a final concentration of 5% formic acid. Digested peptide mixtures were loaded onto a biphasic (strong cation exchange–reverse phase) capillary column and analyzed by two-dimensional liquid chromatography in combination with tandem MS as previously described[22,54]. Peptides were eluted in a five-step MudPIT experiment (using 0%, 25%, 50%, 80% and 100% salt bumps), and data were collected in an LTQ ion trap mass spectrometer (Thermo Scientific) set in a data-dependent acquisition mode with dynamic exclusion turned on (60 s). One full MS survey (ms1) scan was followed by seven ms2 scans. The ms2 spectra data were extracted from the raw file using RAW Xtractor (version 1.9.1) software, which is publicly available (http://fields.scripps.edu/?q=content/download). ms2 spectra data were searched using the SEQUEST algorithm (Version 3.0) against the latest release of the mouse IPI database. The resulting ms2 spectra matches were assembled and filtered using DTASelect (version 2.0.27), and a quadratic discriminant analysis was used to achieve a maximum peptide false positive rate of 1%, as previously described[55,56]. Because comparative quantitation is most accurate when restricted to proteins that show an average of ≥10 spectral counts in at least one of the two groups under comparison[22], this filter was applied. Hierarchical clustering analysis shown in **Figure 1a** was performed using MultiExperiment Viewer (MeV). For each cell line used, the mean of spectral counts for each serine hydrolase across both conditions (preadipocytes and adipocytes; n = 3–4 replicates per condition) was calculated, and this number was used to normalize all individual values. The average of normalized activity for each enzyme in each condition and cell line was then analyzed using MeV_4_8 software[57] (http://www.tm4.org/). Hierarchical clustering analysis of normalized mean enzyme activities was carried out using

doi:10.1038/nchembio.1429

Pearson's correlation coefficient and average linkage. The scale reflects the lower limit (0.0; blue), the midpoint (1.0; black) and the upper limit (2.0; yellow) of normalized mean signals (colors refer to **Fig. 1a**).

***In vitro* serine hydrolase inhibition profiling.** HEK293T or COS-7 cells were transiently transfected using FuGENE 6 (Roche) with expression plasmids for individual serine hydrolases. All of the serine hydrolase cDNAs used were in pCMV-SPORT6 (clones from MGC). Cells were lysed 48 h after transfection, and proteomes were prepared for competitive ABPP analysis as described above.

Click chemistry. Alkyne-labeled proteomes (1 mg/ml in PBS) were incubated with Rh-N_3 (50 µM), followed by TCEP (1 mM), ligand (100 µM) and $CuSO_4$ (1 mM). After 1 h at room temperature, reactions were analyzed by SDS-PAGE and in-gel fluorescence scanning as previously described[29]. For ABPP-MudPIT experiments, the same protocol as above was followed, except biotin-N_3 (200 µM final) was conjugated to alkyne-labeled samples using this procedure in large scale (800 µg proteome per reaction).

Animal studies. Eight-week-old male *db/db* mice (BKS.Cg-*Dock7m* +/+ *Lepr*^{db}/J; JAX stock 000642, The Jackson Laboratory) were randomized into groups on the basis of body weight and blood glucose and dosed orally once per day with 30 mg per kg body weight WWL113, 4 mg per kg body weight rosiglitazone or vehicle (0.5% hydroxypropyl methylcellulose; Fluka). For studies with the diet-induced obesity (DIO) model, C57BL/6J male mice fed a 60 kcal% fat diet (Research Diets D12492i) or the control 10 kcal% fat diet (Research Diets D12450Bi) were purchased from The Jackson Laboratory at 12 weeks of age and kept in their respective diets throughout the studies. DIO mice were dosed as above, except that WWL113 was used at 50 mg per kg body weight. Weight and fasted glucose levels were monitored weekly. Mice were fasted for 16 h before analysis of basal blood chemistry parameters. Animal experiments were conducted in accordance with the guidelines of the Institutional Animal Care and Use Committee of The Scripps Research Institute.

Blood chemistry. Blood samples were collected from anesthetized mice by retro-orbital bleeding or from killed mice by cardiac puncture. Plasma was separated using BD Microtrainer PST tubes with Lithium Heparin. Plasma samples were analyzed using an Olympus AU480 analyzer to quantify triglycerides, nonesterified free fatty acids (NEFA), cholesterol and glucose. Insulin levels were determined using an Ultra Sensitive Rat Insulin ELISA Kit (Crystal Chem Inc.). Ketone bodies were measured using the Wako Autokit Total Ketone Bodies. When measured manually, serum triglycerides were analyzed using the Serum Triglyceride Determination Kit from Sigma, and total cholesterol, NEFA and glucose were measured using kits from Wako (Cholesterol E, HR Series NEFA-HR (2) and Autokit Glucose).

Glucose and insulin tolerance tests. For glucose tolerance tests, mice were fasted for 16 h, and blood was collected from the tail vein before and at timed intervals after an intraperitoneal injection of glucose (1 g per kg body weight). Plasma glucose was measured using a One-touch Ultra glucometer (Johnson & Johnson). For insulin tolerance tests, mice fasted for 4 h were injected intraperitoneally with insulin (1 U per kg body weight; Novolin, Novo Nordisk). Glucose levels were determined before and at timed intervals after injection.

Histology. Liver tissues and brown and white adipose tissues were fixed in Z-Fix (Anatech), dehydrated and embedded in paraffin, and 3-µm-thick (liver, BAT) or 10-µm-thick (WAT) sections were stained with hematoxylin and eosin staining. Cell size was analyzed using ImageJ software.

Quantification of lipid species. Metabolomics experiments were performed in cells and tissues essentially as previously described[58]. Briefly, in the case of cells, they were frozen after 4 h of serum starvation, and cell pellets were extracted in 2:1:1 chloroform/methanol/Tris buffer (pH 8.0) by Dounce homogenization with 10 nmol of the internal standard C12MAGE. The organic layer was removed, dried under N_2 and resuspended in 120 µl of chloroform, and 30 µl was injected into an Agilent 1100-MSD LC-MS. MAGE levels were quantified by measuring the area under the peak and normalized to the C12 MAGE internal standard. For hepatic neutral lipid analysis, livers were homogenized in 6 ml of 2:1 chloroform:methanol and 2 ml of Tris buffer pH 8.0 in the presence of 10 nmol dodecylglycerol and 10 nmol pentadecanoic acid as internal standards. The homogenized mixture was centrifuged at 2,000*g* for 5 min, and the bottom organic layer was collected, dried under N_2 and resolubilized in 120 µl of chloroform. An aliquot of the extract (10 µl) was injected for analysis with an Agilent 6520 Accurate Mass-QTOF-LC/MS. Metabolite separation by liquid chromatography for lipophilic metabolites was achieved using a Gemini reverse-phase C18 column (50 mm × 4.6 mm with 5-µm-diameter particles) from Phenomonex. For diacylglycerol and triacylglycerol analysis, a Luna C5 column (50 mm × 4.60 mm with 5-µm-diameter particles) from Phenomex was used. For LC separation of lipid metabolites, mobile phase A consisted of 95:5 water/methanol and mobile phase B consisted of 60:35:5 isopropanol/methanol/water. Formic acid (0.1%) or ammonium hydroxide (0.1%) was included to assist in ion formation in positive and negative ionization modes, respectively. For diacylglycerol and triacylglycerol analysis, 5 mM ammonium formate was also used in addition to 0.1% formic acid to facilitate positive ionization and NH_4^+ adduct formation. The flow rate for each run started at 0.1 ml/min with 0% B. At 5 min, the flow rate was immediately increased to 0.4 ml/min, and the solvent was increased linearly from 0% to 100% B over 40 min. This was followed by an isocratic gradient of 100% B for 10 min at 0.5 ml/min before equilibrating for 5 min at 0% B at 0.5 ml/min. The data files were exported as mzData files and subjected to XCMS analysis to identify metabolites that were significantly ($P < 0.05$) different between vehicle and WWL113-treated tissues. Neutral lipid (di- and triacylglycerols were extracted as NH_4^+ adducts) masses (identified by exact mass and coelution with standard of one lipid species within each class of lipid analyzed) were manually extracted and quantified by measuring the area under the peak in relation to an internal standard and an external standard curve of the metabolite compared to the internal standard.

Human samples. Abdominal subcutaneous adipose tissue was obtained from anaesthetized subjects undergoing bariatric surgery. The tissue was snap-frozen in liquid nitrogen and stored at –80 °C. The Monash University Human Research Ethics Committee approved the human experiments, and informed consent was obtained from patients before surgery.

Statistics. Analyses were performed with the Student's *t*-test for independent samples. Data is expressed as mean ± s.e.m. or s.d. as indicated in the individual legends. A *P* value of less than 0.05 was considered significant. Statistical analyses were performed using GraphPad Prism 5 (GraphPad Software).

Compound synthesis. Chemical synthesis and compound characterization are described in the **Supplementary Note**.

51. Patricelli, M.P., Giang, D.K., Stamp, L.M. & Burbaum, J.J. Direct visualization of serine hydrolase activities in complex proteomes using fluorescent active site-directed probes. *Proteomics* **1**, 1067–1071 (2001).
52. Liu, Y., Patricelli, M.P. & Cravatt, B.F. Activity-based protein profiling: the serine hydrolases. *Proc. Natl. Acad. Sci. USA* **96**, 14694–14699 (1999).
53. Kidd, D., Liu, Y. & Cravatt, B.F. Profiling serine hydrolase activities in complex proteomes. *Biochemistry* **40**, 4005–4015 (2001).
54. Washburn, M.P., Wolters, D. & Yates, J.R. III. Large-scale analysis of the yeast proteome by multidimensional protein identification technology. *Nat. Biotechnol.* **19**, 242–247 (2001).
55. Cociorva, D., Tabb, D.L. & Yates, J.R. Validation of tandem mass spectrometry database search results using DTASelect. *Curr. Protoc. Bioinformatics* **16**, 13.04 (2007).
56. Tabb, D.L., McDonald, W.H. & Yates, J.R. III. DTASelect and Contrast: tools for assembling and comparing protein identifications from shotgun proteomics. *J. Proteome Res.* **1**, 21–26 (2002).
57. Saeed, A.I. *et al.* TM4: a free, open-source system for microarray data management and analysis. *Biotechniques* **34**, 374–378 (2003).
58. Nomura, D.K. *et al.* Endocannabinoid hydrolysis generates brain prostaglandins that promote neuroinflammation. *Science* **334**, 809–813 (2011).